Structure of small silver clusters and static response to an external electric field

M. Pereiro* and D. Baldomir

Instituto de Investigacións Tecnolóxicas and Departamento de Física Aplicada, Universidade de Santiago de Compostela,
E-15782 Santiago de Compostela, Spain

The static response properties and the structural stability of silver clusters in the size range $1 \leq n \leq 23$ have been studied using a linear combination of atomic Gaussian-type orbitals within the density functional theory in the finite field approach. The Kohn-Sham equations have been solved in conjunction with a generalized gradient approximation (GGA) exchange-correlation functional. A proof that the finite basis set GGA calculation satisfies the Hellmann-Feynman theorem is also included in the Appendix. The calculated polarizabilities of silver clusters are compared with the experimental measurements and the jellium model in the spillout approximation. Despite the fact that the calculated polarizabilities are in good agreement with both of them, we have found that the polarizability appears to be strongly correlated to the cluster shape and the highest occupied–lowest unoccupied molecular-orbital gap.

I. INTRODUCTION

Transition-metal clusters play a dominant role in cluster physics [1]. They have attracted the interest of many researchers and consequently the number of publications on that topic have experienced a dramatic increase over the past thirty years because metal clusters exhibit increasingly interesting structural, electronic, catalytic, as well as optical properties [2,3]. Likewise, the biomedical applications of nanoclusters have experienced a great impact in the biomedicine community [4].

Among the aforementioned applications and properties of metal clusters, their optical properties that result from the light-matter interaction at the nanoscale level are an area of great current interest [5]. Many of the advances in this area could not have been made possible without the development of the optical spectroscopy techniques that have been indispensable for elucidating the electronic structure of clusters. These experimental techniques can be divided into two groups, that is, nondestructive and destructive methods. In the former methods, also called linear response methods, a weak electromagnetic field interact with the cluster and it absorbs or scatters light without undergoing ionization or dissociation, whereas in the destructive methods the ionization is achieved. The nondestructive methods in connection with the linear-response theory have been extensively used to calculate photoabsorption cross sections and specially static dipole polarizabilities.

The static dipole polarizability is a physical observable of metal clusters that has been shown to be closely related to the shape and structural geometry. For example, electronic structure calculations of small Si clusters show that the polarizability is strongly correlated with the shape of the clusters [6]. Likewise, the interplay between theory and experiment is a powerful tool that serves to identify which cluster is observed in the experiments throughout the comparison of the calculated polarizabilities with the experimental ones [7].

Moreover, the static dipole polarizability is also well known to be intimately related to the shell electronic structure. For example, the noble-metal clusters whose optical properties have been extensively studied in literature (mainly from the experimental side) present lower static polarizabilities than alkali metals because they are excellent examples of spherical shell structure. However, in the case of the silver clusters, the influence of d electrons in the static polarizability has been less studied at least from the theoretical point of view and it deserves more investigation. This point, among others, is addressed in this work.

In this article we have employed a density functional theory-based (DFT) calculation within the generalized gradient approximation (GGA) to properly account for the strong correlation effect of the localized d electrons and charge density inhomogeneities. We have studied the structural stability and the static response properties of small silver clusters ranging in size from $n=1$ up to $n=23$, where n is the number of atoms forming the cluster. The calculated static polarizabilities are only compared with the available experimental data since, unfortunately, no *ab initio* quantum-molecular calculations have been done so far for the static polarizabilities of silver clusters in the size range covered by our investigation. The available theoretical data are reported in Ref. [8] for very small silver clusters with $1 \leq n \leq 8$. The agreement between our values and those of Idrobo *et al.*, who computed the static polarizabilities within the framework of the real space finite-difference *ab initio* pseudopotential method, is excellent in the case of the GGA approximation, which makes the results obtained with the present DFT method more valuable. In addition, we have compared our results with the jellium model in the spillout approximation and the deviation of our results from this model is explained in terms of the electronic structure parameters like highest occupied and lowest unoccupied molecular orbital (HOMO-LUMO) gaps or structural symmetry. We also show and discuss how the d electrons affect the static polarizabilities since when n is sufficiently large, i.e., greater than 18, the polarizability tends to be constant in contrast to the one of the alkali metals. The rest of the paper is organized as follows. In Sec. II, we present the theoretical background and

---

*Electronic address: fampl@usc.es

the computational details along with the computational parameters used in this article. Moreover, the structural stability of the silver clusters is studied in detail in Sec. III. The results of our calculations and the influence of the electronic structure observables in the static polarizabilities are given in Sec. IV. We conclude with a brief summary of the reported results provided by our *ab initio* calculations in Sec. V. In the Appendix we prove that the Hellmann-Feynman theorem is satisfied by the finite basis set density functional framework in the generalized gradient approximation.

II. METHOD AND COMPUTATIONAL DETAILS

Traditionally there has been two different ways of computing the polarizability of molecular systems. Thus the polarizability is identified either as the second-order term in the perturbation expansion of the electronic energy with respect to the applied external uniform electric field or as the linear response of the dipole moment to that electric field. Both definitions are equivalent when the Hellmann-Feynman theorem is satisfied. The Hellmann-Feynman theorem holds for an exact solution of the Schrödinger equation and also for some approximate solutions. In particular, it is satisfied by the fully self-consistent finite basis set solutions when the exchange-correlation (XC) energy is approximated by the GGA as shown in the Appendix.

We have adopted the dipole-moment-based definition as our working definition because in this expression the field occurs only in the first power for the calculation of the polarizability instead of the second as in the energy expansion. The polarizabilities α_{ij} ($\{i,j\}=x,y,z$ or alternatively $\{i,j\}=1,2,3$) are calculated by the finite field (FF) method [9] which consists of computing the electric dipole moment μ_i of a system under the influence of an external electric field F_i according to the following finite-difference relation:

$$\alpha_{ij} = \left(\frac{\partial \mu_i(F_j)}{\partial F_j} \right)_{\vec{F}=0} = \lim_{F_j \to 0} \frac{\mu_i(F_j) - \mu_i(-F_j)}{2F_j}. \quad (1)$$

In the FF method, one of the most crucial problems to evaluating the derivatives is the choice of an appropriate field strength. Several works have assessed the numerical accuracy of polarizability against different field values and concluded that the best region of linear response is for field strengths ranging from 10^{-4} up to 10^{-2} a.u. [10,11]. For that reason we have used a field strength of 5×10^{-4} a.u. that is applied along the molecular axis. At least seven self-consistent field (SCF) runs, with the field strengths 0 and $\pm F_i$, are necessary to calculate the polarizability. Once the polarizability tensor components are computed, the mean static polarizability is calculated as $\bar{\alpha} = (\Sigma_{i=1}^{3} \alpha_{ii})/3$ and the polarizability anisotropy is defined as

$$\Delta\alpha = \sqrt{\frac{\displaystyle\sum_{\substack{i,j=1,2 \\ i<j}}^{2,3} (\alpha_{ii} - \alpha_{jj})^2 + 6 \sum_{\substack{i,j=1,2 \\ i<j}}^{2,3} \alpha_{ij}^2}{2}} \quad (2)$$

in the general axis frame or without the second addended $(6\Sigma_{i,j=1,2;i<j}^{2,3}\alpha_{ij}^2)$ in the coordinate system which makes the second-rank polarizability tensor α diagonal.

With the aim of studying the static response properties of small silver clusters, Ag_n ($2 \le n \le 23$), we have performed density functional theory-based calculations consisting of a linear combination of Gaussian-type-orbitals (LCGTO) Kohn-Sham density-functional methodology as it is implemented in the DEMON-KS3P5 program [12]. All-electron spin-unrestricted calculations were carried out at the GGA level to take the XC effects into account [13]. Local-density approximation (LDA) sometimes yields inaccurate bond lengths and total energies due to the insufficiency in describing the strong correlation effects of the localized d electrons and charge density inhomogeneities. In these regards, the GGA should be a better choice than LDA [14]. For this reason, at the beginning of this work and to satisfy ourselves that the numerical procedure is reliable, we initiate a search of the functional that better fitted the calculated bond length of the silver dimer to the experimental one. The functional developed by Perdew and Wang [13] gave us a bond length of 2.534 Å that is in excellent agreement with the experimental measure (2.53350 Å) reported in Ref. [15]. An orbital basis set of contraction pattern (633321/53211*/531+) was used in conjunction with the corresponding (5,5;5,5) auxiliary basis set for describing the s, p, and d orbitals [16]. In DEMON-KS3P5, the electron density is expanded in auxiliary basis functions which are introduced to avoid the calculation of the N^4 scaling Coulomb repulsion energy, where N is the number of the basis functions. The grid for numerical evaluation of the XC terms had 128 radial shells of points and each shell had 26 angular points. Spurious one-center contributions to the XC forces, typically found in systems with metal-metal bonds when using a nonlocal functional, are eliminated in a way similar to what has been done in Ref. [17]. A wide set of spin multiplicities ranging from 1 to 11 was checked to ensure that the lowest-energy electronic configuration is reached. The geometries were fully optimized without symmetry and geometry constraints using the Broyden-Fletcher-Goldfarb-Shanno algorithm [18]. During the optimization, the convergence criterion for the norm of the energy gradient was fixed to 10^{-4} a.u. while it was 10^{-7} a.u. for the energy and 10^{-6} a.u. for the charge density. The ground state structures and some of the lowest-energy isomers of the silver clusters studied in this article are illustrated in Fig. 1, since that the polarizability is closely related to the geometrical shape of the cluster.

III. STRUCTURES OF SILVER CLUSTERS

Figure 1 and Table I show the structures, relative energies, first-neighbor distances, and vertical ionization potentials (IP) of the lowest-energy isomers predicted by the simulations for Ag_n clusters with $2 \le n \le 23$. The IPs have been calculated as the energy difference between the neutral cluster and the cation. We assign labels to clusters such as n_m, where n indicates the number of atoms and the second number gives the rank in increasing energy order. A huge sampling of trial geometries taken from the literature was evaluated [19]. While for these small clusters, it is nearly impossible to search for all possible geometries, the detailed search that we have carried out gives us some confidence that the ground state structures have been found.
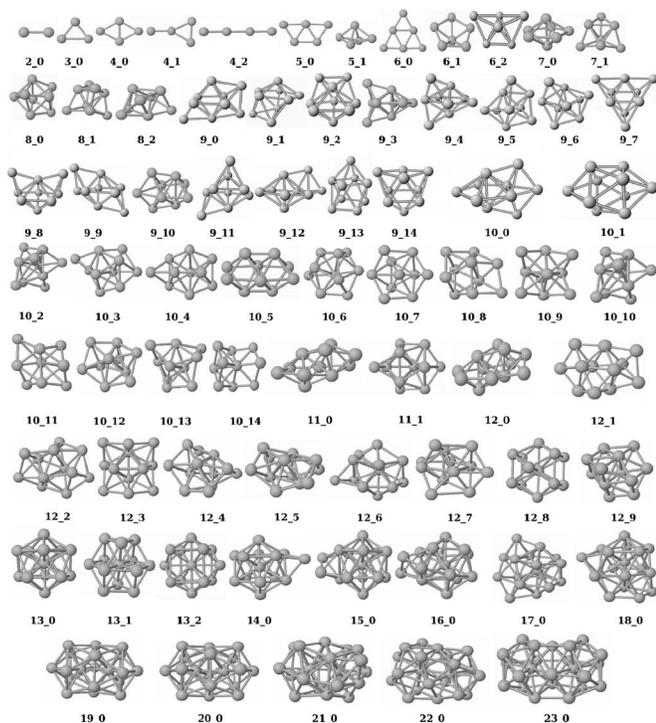
FIG. 1. Lowest-energy structures and isomers of Ag_n, $n=2-23$, ordered (from left to right and top to bottom) by increased size and energy. The cluster n_m is the mth energetic isomer with n atoms.

For clusters with size varying from 2 up to 13, we optimized geometries and calculated energies for 78 isomers. We only reported the lowest-energy structures here, but their Cartesian coordinates in Bohr units are available upon request to the authors. We focus on isomers located 50 KJ/mol (≈ 0.5 eV) or less above the lowest-energy structure because this value is considered to represent an error bar for relative energies computed with GGA functionals [20]. Whenever possible we compare the calculated IPs with the experimental ones to rule out the possible candidates to the ground state geometry. We will focus our attention mainly on the lowest energy cluster geometries which are different form the cluster structures reported in previous experimental or theoretical studies. For the rest of clusters, we simply just describe the lowest energy structures. In Table I, other low energy isomers are also listed for comparison.

For the clusters with size varying from 14 up to 23, we took the initial guess structures from Ref. [21]. Moreover, in the early stage of the geometry optimization process and with the aim of speeding up the calculations, the structure of the silver clusters was first optimized in conjunction with a 17-electron scalar relativistic model core potential designed for the adequate description of the silver dimer bond length [22]. Once the geometry of the cluster was converged for the model core potential, an all-electron structural-relaxation calculation was performed leading to the current lowest-energy structures showed in Fig. 1.

For the silver trimer, we have studied only one structure (isosceles triangle) because the minimum structure is well established in the literature [19,23]. In the case of Ag_4, the lowest energy structure that we have found is the planar

rhombus. The lowest-energy structures for Ag_3 and Ag_4 predicted by our calculations are in good agreement with other *ab initio* results [19,23,24].

The ground state structure found for the pentamer is a trapezoid with C_{2v} symmetry. In literature there is a controversy about the assignment of the structural minimum. Some theoretical studies predict as the ground state the planar structure [19,24,25] while other ones predict the trigonal bipyramid [23]. On the experimental side, it is worthwhile to mention that different experimental electron spin resonance and Raman spectra of Ag_5 have been interpreted by both trigonal bipyramid [26] and planar geometries [27], respectively. As shown in Table I, the vertical IP calculated for the trapezoid agrees quite well with the experimental result [28] and it is what underpins our predicted lowest-energy structure.

Four structures have been optimized for the Ag_6 cluster [29]. The planar trapezoidal D_{3h} structure resulted to be the most stable but only 0.079 eV lower in energy than the pentagonal pyramid. Both structures exhibit IPs very close to the experimental one and therefore, our *ab initio* calculations do not allow prediction of only one geometry as the structural minimum.

In the case of the silver heptamer, the pentagonal bipyramid (D_{5h} symmetry) is predicted as the lowest energy structure while the tricapped tetrahedron is 0.17 eV higher in energy. Although the relative energy and the ionization potentials do not allow a clear prediction about the minimum geometry, however most of the first principles calculations prior to this article have also obtained the pentagonal bipyramid as the fundamental structure [8,19,23,24,30].

For the silver octamer, we have decided to optimize as a good candidate to the structural minimum the following isomers: A D_{2d} dodecahedron, which can be viewed as a distorted bicapped octahedron, a T_d tetracapped tetrahedron, and a C_s pentagonal bipyramid. Our calculations stabilize first the dodecahedron, secondly but very close in energy the T_d structure and finally the pentagonal bipyramid with $\Delta E_{DFT}=0.181$ eV. The comparison between the calculated IPs and the experimental measurements reported in Ref. [28] favor more the T_d structure than the D_{2d} one, however the assignment of the structural minimum is clearly inverted if we use the experimental IP (6.40 eV) measured in Ref. [31]. Our predicted minimum structure is also supported by a very recent reference where the authors determine the lowest-energy structure of Ag_8 by comparison of the optical spectra provided by time-dependent DFT with the experimental findings [32].

Fifteen structures have been optimized in the case of the Ag_9 cluster. A tricapped-distorted octahedron (C_s) was found for the lowest-energy structure which is in good agreement with the reported structure in Ref. [19], while in Refs. [23,24] the ground state geometry is the bicapped pentagonal bipyramid. To satisfy ourself that the bicapped pentagonal bipyramid is not the structural minimum, we studied a wide range of pentagonal bipyramid structures capped with two atoms in different positions. After the geometry optimization, the final geometry is slightly distorted in most of the cases. The structures are plotted in Fig. 1 and denoted as 9_1, 9_2, 9_3, 9_4, 9_5, 9_6, 9_8, 9_9, 9_10, 9_11, and 9_12. It

TABLE I. Average first-neighbor distance and relative energy of Ag_n cluster isomers with $2 \leq n \leq 23$. The vertical ionization potential is compared with the data from Ref. [28]. The geometry notation is that of Fig. 1.

			$Ag_2 \mapsto Ag_{10\_4}$						$Ag_{10\_5} \mapsto Ag_{23\_0}$		
				Vertical IP						Vertical IP	
Cluster	d (Å)	ΔE_{DFT} (eV)	Calc. (eV)	Expt. (eV)	$\|\Delta IP\|$ (eV)	Cluster	d (Å)	ΔE_{DFT} (eV)	Calc. (eV)	Expt. (eV)	$\|\Delta IP\|$ (eV)
2_0	2.53	0.000	7.73	7.60	0.13	10_5	2.78	0.397	6.63	6.25	0.38
3_0	2.79	0.000	5.67	6.20	0.53	10_6	2.81	0.495	6.26	6.25	0.01
4_0	2.71	0.000	6.54	6.65	0.11	10_7	2.81	0.506	6.24	6.25	0.01
4_1	2.63	0.242	6.51	6.65	0.14	10_8	2.78	0.553	6.36	6.25	0.11
4_2	2.56	0.563	6.93	6.65	0.28	10_9	2.77	0.617	5.99	6.25	0.26
5_0	2.72	0.000	6.33	6.35	0.02	10_10	2.78	0.626	6.04	6.25	0.21
5_1	2.77	0.430	6.16	6.35	0.19	10_11	2.74	0.703	6.34	6.25	0.09
6_0	2.72	0.000	7.22	7.15	0.07	10_12	2.80	0.720	6.00	6.25	0.25
6_1	2.72	0.079	7.09	7.15	0.06	10_13	2.79	1.151	6.14	6.25	0.11
6_2	2.80	0.534	6.67	7.15	0.48	10_14	2.75	1.133	5.90	6.25	0.35
7_0	2.79	0.000	6.36	6.40	0.04	11_0	2.81	0.000	6.66	6.30	0.36
7_1	2.76	0.170	6.44	6.40	0.04	11_1	2.81	0.268	6.32	6.30	0.02
8_0	2.80	0.000	6.44	7.10	0.66	12_0	2.82	0.000	7.01	6.50	0.51
8_1	2.76	0.006	7.33	7.10	0.23	12_1	2.79	0.117	6.91	6.50	0.41
8_2	2.78	0.181	6.66	7.10	0.44	12_2	2.80	0.161	6.72	6.50	0.22
9_0	2.80	0.000	6.53	6.00	0.53	12_3	2.81	0.411	6.65	6.50	0.15
9_1	2.81	0.039	5.83	6.00	0.17	12_4	2.81	0.417	6.50	6.50	0.00
9_2	2.81	0.039	5.97	6.00	0.03	12_5	2.81	0.422	6.49	6.50	0.01
9_3	2.78	0.052	5.72	6.00	0.28	12_6	2.81	0.652	6.42	6.50	0.08
9_4	2.78	0.056	5.83	6.00	0.17	12_7	2.80	0.802	6.36	6.50	0.14
9_5	2.78	0.070	5.91	6.00	0.09	12_8	2.80	1.039	6.58	6.50	0.08
9_6	2.77	0.089	5.99	6.00	0.01	12_9	2.71	1.039	6.53	6.50	0.03
9_7	2.78	0.145	5.77	6.00	0.23	13_0	2.87	0.000	5.75	6.34	0.59
9_8	2.79	0.154	5.70	6.00	0.30	13_1	2.72	0.305	6.23	6.34	0.11
9_9	2.75	0.182	6.45	6.00	0.45	13_2	2.62	3.568	5.88	6.34	0.46
9_10	2.77	0.204	6.31	6.00	0.31	14_0	2.83	0.000	5.87	6.73	0.86
9_11	2.79	0.211	5.86	6.00	0.14	15_0	2.83	0.000	5.82	6.40	0.58
9_12	2.78	0.214	6.55	6.00	0.55	16_0	2.82	0.000	5.79	6.57	0.78
9_13	2.77	0.218	6.11	6.00	0.11	17_0	2.82	0.000	5.84	6.45	0.61
9_14	2.77	0.221	5.91	6.00	0.09	18_0	2.82	0.000	5.95	6.53	0.58
10_0	2.82	0.000	6.58	6.25	0.33	19_0	2.85	0.000	5.35	6.20	0.85
10_1	2.77	0.080	7.27	6.25	1.02	20_0	2.85	0.000	5.39	6.45	1.06
10_2	2.78	0.158	6.68	6.25	0.43	21_0	2.84	0.000	5.36	5.90	0.54
10_3	2.79	0.205	6.51	6.25	0.26	22_0	2.82	0.000	5.56	6.04	0.48
10_4	2.78	0.221	6.77	6.25	0.52	23_0	2.84	0.000	5.42	6.03	0.61

is worthwhile to mention that from 9_0 up to 9_6, the structures are very close in energy and only the IPs of the pentagonal bipyramid structures agrees quite well with the experimental ones, so in gas-phase experiments is likely to obtain the bicapped pentagonal bipyramid as the lowest-energy structure.

Contrary to what happened in the case of nanomers, the lowest-energy geometry of Ag_{10} cluster is a pentagonal

bipyramid-shaped structure, namely, a tricapped pentagonal bipyramid. With the aim of testing the validity of this structure, we have also optimized a very distorted pentagonal bipyramid but it finally converged to the 10_0 structure. The second structure is a D_{4d} bicapped square antiprism and it is only 0.080 eV higher in energy with respect to the ground state. This structure has been predicted as the fundamental one in Ref. [23], nevertheless the comparison of the calcu-

lated IPs reported in Table I with the experimental value clearly show that the 10_0 structure is the best candidate to be the minimum structure.

The guess structures for Ag_{11} and Ag_{12} were obtained by adding atoms to the pentagonal bipyramid structure or by removing them from a 13-atom O_h cuboctahedron or from the icosahedral packing. Thus, the lowest-energy structures come from the pentagonal bipyramid shape in both cases while the structures coming from the cuboctahedron or the icosahedral packing are less favored energetically. In the case of the Ag_{11} geometries, we have studied nine isomers but, except for the 11_1 structure, the other ones are energetically far from the lowest-energy structure by an amount greater than 0.5 eV. While the relative energies clearly show that the fundamental structure is the one labeled with 11_0 ($\Delta E_{DFT}^{11\_0 \rightarrow 11\_1} = 0.268$ eV), however the calculated IP ($\Delta IP^{11-1} = 0.02$ eV) predicts the 11_1 as the minimum structure, and consequently these two structures would be probably observed in experiments. The same situation occurs for Ag_{12} but in this case more structures can be observed in low-temperature experiments.

Three structures have been selected as possible candidates for the structural minimum of the thirteen-atom silver cluster. They are the icosahedral geometry (I_h symmetry), the cuboctahedron cluster (O_h symmetry), and the D_{2h} structure which is a compact portion of the bcc crystal lattice capped with four atoms as it is illustrated in Fig. 1. After the relaxation of the structures, the ground state geometry predicted by our calculations is the icosahedral structure. Although the calculated IPs are in general in a relatively good agreement with the experimental ones, however they do not add too much information to the determination of the lowest-energy structure. The relative energies of the isomers collected in Table I together with the fact that most of the articles devoted to the study of the structural properties of small silver clusters predict the icosahedral structure as fundamental one, give us some confidence that the icosahedral packing is valid for the Ag_{13} cluster [23,33,34].

As we commented above, for the rest of the clusters, that is, from Ag_{14} up to Ag_{23} we took the initial guess structures from Ref. [21]. They follow an icosahedral growth sequence capped with a variable number of atoms depending on the cluster size. In general, the calculated IPs are in good agreement with the experimental measurements which make more valuable the geometries optimized with the DEMON-KS3P5 program using as starting point the structures predicted in Ref. [21].

IV. RESULTS AND DISCUSSION

The main results of our theoretical calculations concerning the static response properties in conjunction with some selected electronic structure properties of small silver clusters are collected in Table II and Fig. 2. Hereafter, the reported results are only for the ground state structures. We observe that the calculated polarizabilities are in good agreement with the experimental measurements reported in Ref. [35]. They approach each other as the cluster size increases because the experimental data are less reliable as the cluster

TABLE II. Calculated static response and electronic structure properties of the lowest-energy DFT-optimized Ag_n clusters. The disproportionation energy is denoted by $\Delta_2 E_n$ and $\Delta \xi$ stands for the HOMO-LUMO gap. The mean static polarizability per atom $\bar{\alpha}_{at}$ and the polarizability anisotropy per atom $\Delta \alpha_{at}$ were calculated under the influence of an external electric field of strength 0.0005 a.u. The absolute value of the dipole moment is denoted by μ.

Cluster	Symmetry	$\Delta_2 E_n$ (eV)	$\Delta \xi$ (eV)	$\bar{\alpha}_{at}$ (Å³/atom)	$\Delta \alpha_{at}$ (Å³/atom)	μ (D)
1_0			1.24	6.85	0	0.06
2_0	$D_{\infty h}$	0.74	2.08	6.88	6.33	0.18
3_0	C_{2v}	−0.97	0.70	7.86	7.21	0.58
4_0	D_{2h}	0.28	0.89	7.15	7.83	0.13
5_0	C_{2v}	−0.56	0.55	7.35	6.74	0.17
6_0	D_{3h}	0.43	2.19	7.15	5.69	0.17
7_0	D_{5h}	−0.42	0.43	6.47	2.07	0.30
8_0	D_{2d}	0.79	1.72	6.32	1.22	0.46
9_0	C_s	−0.73	0.37	6.62	3.49	0.54
10_0	D_{2d}	0.43	0.97	6.54	3.99	0.77
11_0	C_1	−0.47	0.28	6.51	4.05	0.41
12_0	C_s	1.21	0.83	6.41	3.73	0.60
13_0	I_h	−0.73	0.62	5.96	0.02	0.66
14_0	C_{3v}	−0.16	0.43	5.75	1.25	0.76
15_0	C_{2v}	−0.02	0.26	5.69	1.56	1.20
16_0	C_s	−0.05	0.21	5.62	1.53	1.18
17_0	C_2	0.17	0.20	5.56	1.51	1.32
18_0	C_s	1.11	0.65	5.53	1.66	0.94
19_0	D_{5h}	−1.10	0.12	5.67	2.22	1.15
20_0	C_{2v}	0.33	0.09	5.73	1.66	1.16
21_0	C_1	0.21	0.15	5.73	1.45	0.94
22_0	C_s	0.12	0.14	5.62	1.80	1.93
23_0	D_{3h}		0.19	5.84	3.06	1.52

size decreases. The polarizabilities reported by Fedrigo *et al.* [35] were measured at $T=10$ K whereas our calculated results are given at $T=0$ K. Thus, according to the following relation [36] in the low electric field limit

$$\alpha_{eff} = \bar{\alpha} + \frac{\mu^2}{3k_B T} \tag{3}$$

for clusters having a permanent dipole moment μ, the effective measured polarizability at temperature T is expected to be greater than average polarizability. However we have found that the contribution of the second term in Eq. (3)—calculated at $T=10$ K and for the dipole moments collected in Table II—is negligible and consequently the influence of the temperature in the confrontation of the calculated polarizabilities and the experimental results can be considered of less importance. It is worth to note that the theoretical polarizabilities oscillate and manifest a decreasing trend such as the experimental values do. It converts the experimental setup designed by Fedrigo *et al.* in a valuable technique to study the electronic properties of small silver clusters.
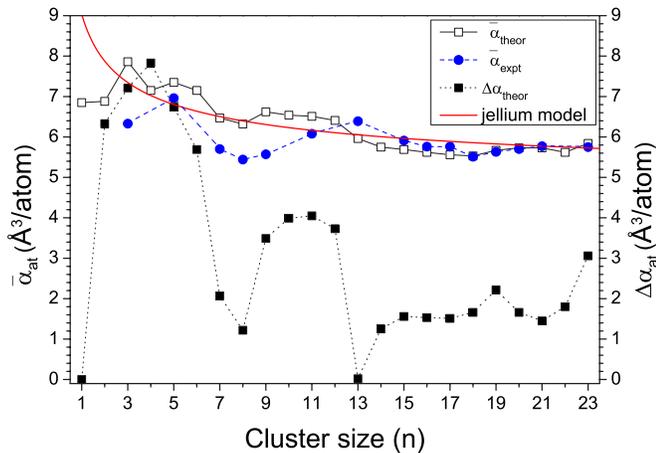
FIG. 2. (Color online) Mean static polarizabilities per atom (open squares) and the polarizability anisotropies per atom (solid squares) of Ag_n clusters calculated with the FF method as a function of the cluster size. The solid circles represent the experimental measurements of the polarizabilities per atom taken from Ref. [35]. The solid line represents the prediction from the jellium model. The fitted parameters are given in the text.

In Fig. 3, we have plotted the average bond length of the lowest-energy structures collected in Table I versus the cluster size. We have observed an abrupt change of the first-neighbor distance from Ag_2 to Ag_3 and from Ag_6 to Ag_7, which is in our opinion a consequence of the structural transition from one dimension (1D) to 2D and from 2D to 3D, respectively. The structural transition clearly affects the static polarizabilities, as we will see below. Moreover, we can see that in general the average bond length approaches to the experimental value of equilibrium interatomic distance of fcc silver solid (2.89 Å) as the cluster size gets bigger [37]. It is
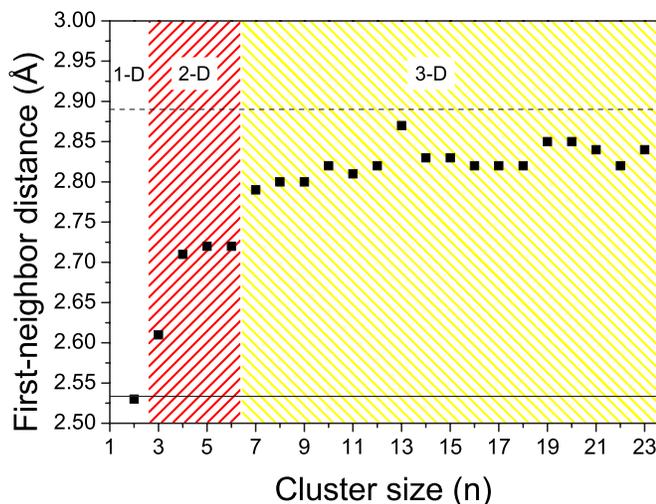
FIG. 3. (Color online) First-neighbor distance plotted against the cluster size. The solid line represents the experimental silver dimer bond length and the dashed line symbolizes the experimental value of the equilibrium interatomic distance of fcc silver bulk. The three different areas stand for the one-dimensional (1D), bidimensional (2D), and three-dimensional (3D) lowest-energy structures of the small silver cluster, respectively.

a consequence of the very important role of the surface effects in small clusters where most of the atoms belong to the surface.

As far as the static polarizabilities displayed in Fig. 2 is concerned, we observe an odd-even oscillation of the calculated polarizability per atom in function of the cluster size ranging from the dimer up to the hexamer. This fact is characteristic of clusters of atoms with an odd number of electrons and specially for atoms with a closed d shell and a single valence electron like in the case of noble-metals (Cu, Ag, and Au), or the closely related alkali metals (Li, Na) [38]. The even-odd oscillation of the polarizability up to the hexamer is due to the even-odd oscillation of the HOMO-LUMO gap (see Table II in conjunction with the symmetry of the ground state geometries). Roughly speaking an increase of the HOMO-LUMO gap is on the side of a chemical stabilization of the cluster but the chemical stability is favored by three-dimensional spherical structures or highly symmetric two-dimensional geometries which lead to a lost of the static polarizability. It is clearly reflected in Fig. 4(a), where clusters with small HOMO-LUMO gaps have larger polarizability than those with large gaps. Thus, the static polarizability oscillates inversely as HOMO-LUMO gap does. The odd-even oscillating trend is broken at $n=7$ because of the shape transition from the planar to the compact three-dimensional structures and is reflected by a significant decrease in the polarization of Ag_7 despite the fact that the HOMO-LUMO gap decrease in relation to Ag_6 and Ag_8. In this case, the symmetry of the structure dominates over the HOMO-LUMO gap.

From $n=7$ up to $n=18$, the static polarizability decreases smoothly in accordance with the expectation that the polarizability per atom of a cluster is a quantity that decreases as the cluster becomes more compact and symmetric. It is borne out by the results displayed in Fig. 4(b) and the inset of Fig. 4(a). With this purpose, we have defined the parameter γ that characterizes the geometry as

$$\gamma = \frac{5 \operatorname{tr} \mathbf{I}}{6na^2}, \qquad (4)$$

where tr $\mathbf{I}$ is the trace of the moment of inertia tensor of the clusters relative to the principal axis frame, n is the number of atoms of the cluster, and a stands for the radius of the silver atom ($a \approx 1.45$ Å). In Fig. 4(b) it is shown that the larger clusters tend to have higher γ because they are structurally more elongated and consequently it is consistent with the classical picture that the more spherically symmetric the cluster is, the less polarizable it is. An exception is found for Ag_7 and Ag_{13} but the reason will be commented on below in the case of Ag_{13} because for Ag_7 the structure determines the reduction of the polarizability as stated above. Despite the fact that the geometry is a fundamental parameter to describe the polarizability, it is, however, not the only one. It is necessary to take into account the influence of the HOMO-LUMO gap. Generally, the polarizability is a result of the competition between the former and the latter contributions, as is shown in Fig. 4. Two structures (Ag_8 and Ag_{13}) manifest a significant reduction of the polarizability that is clearly
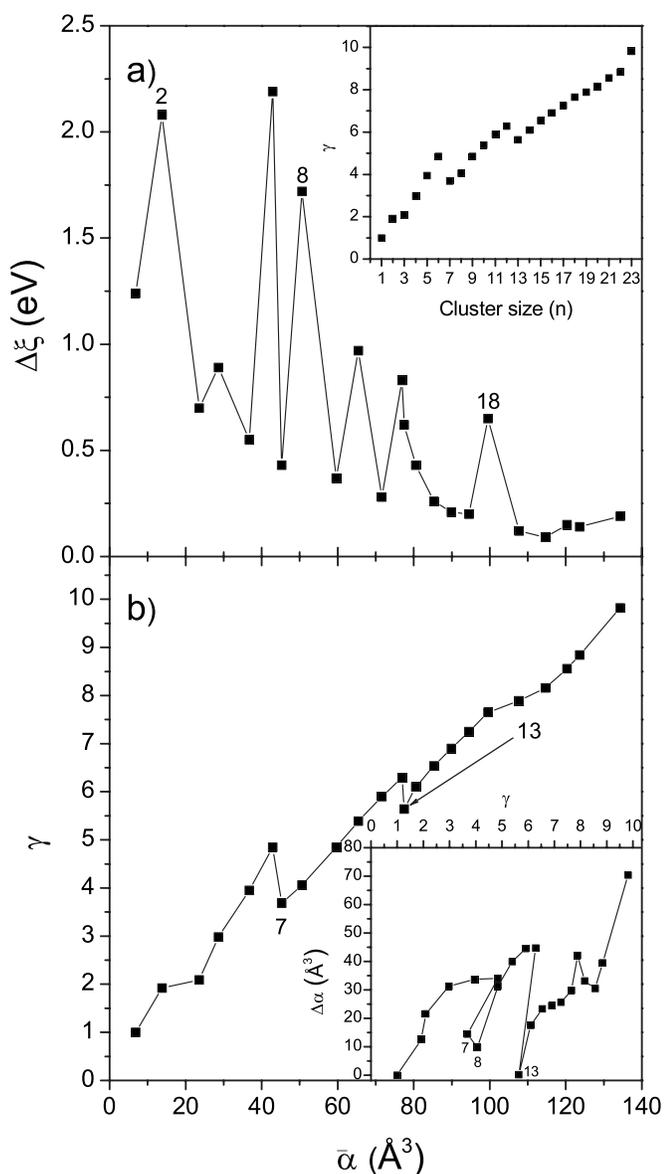
FIG. 4. (a) The calculated HOMO-LUMO gap $\Delta\xi$ and (b) the normalized moment of inertia γ plotted against the mean static polarizability. The inset in the upper panel shows the evolution of the normalized moment of inertia versus the cluster size. In the bottom panel, the inset compares the polarizability anisotropy with γ.

FIG. 5. (Color online) Evolution of the partial density of states of the higher-lying occupied and lower-lying unoccupied levels with the cluster size. The solid, dashed, and dotted lines represent the contribution of the $5s$, $5p$, and $4d$ orbitals to the total density of states, respectively. The dotted vertical line represents the Fermi level.

reflected in the polarizability anisotropy which measures the symmetry or more specifically the deformation of the charge distribution under the influence of an external electric field in such a way that the less the polarizability anisotropy is, the more spherically symmetric the charge distribution is [see the inset of Fig. 4(b)]. Thus the polarizability anisotropy for Ag$_8$ and Ag$_{13}$ is clearly reduced since that Ag$_8$ is a closed-shell cluster with a large HOMO-LUMO gap and Ag$_{13}$ condensates in a highly symmetric structure, i.e., the icosahedral structure (I_h). The transition from Ag$_8$ to Ag$_9$ is accompanied by an enhancement of the polarizability. It is caused by the level structure since whenever a new level starts to fill, the large spatial extent of the new wave function contributes to

the enhancement of the polarizability [39]. That is the reason for the reduced value of the polarizability in the case of the closed-shell structures with $n=2$, 8, and 18.

From $n=19$ up to $n=23$, the mean static polarizability exhibits a trend with a small positive slope. It has been already found in Ref. [35]. Fedrigo *et al.* speculates that this tendency is due to the ever increasing role of the d electrons as the cluster size grows. They state that a shift to red of the plasmon resonance due to d interband transitions corresponds to an enhancement of the polarizability. Our DFT calculations confirm this argument and the very important role of the d electrons as the cluster increases in size. In Fig. 5, we show the evolution of the partial density of states with the cluster size. Both d and sp levels gradually broaden and overlap with each other approximating to an electronic band in the bulk limit. With the aim to clarify the important role of

d electrons with the size evolution, we have defined the energy separation Δ_{sd} as the difference between highest occupied molecular orbitals belonging to 4*d* states and the lowest occupied molecular orbitals from 5*s* states. The energy separation decreases rapidly from 1.94 eV for Ag_2 to 0.31 eV for Ag_6. The structural transition from planar geometry to a three-dimensional structure gives rise to an increase of the value of Δ_{sd} up to 2.15 eV for Ag_7. After that, it decreases very rapidly up to 0.07 eV for Ag_{14}. For clusters ranging in size from $n=15$ up to $n=23$, the influence of 4*d* level is so important that it merges into the 5*s* state. Moreover, the small HOMO-LUMO gap collected in Table II for *n* = 19–23 compared to smaller clusters favors the slight increase of the mean static polarizability per atom as was commented above.

It is expected that the jellium model can be applied to silver clusters because the electronic configuration of silver is similar to the alkali clusters, where the jellium model has been successfully applied. The solid line in Fig. 2 symbolizes the polarizability predicted by the jellium model. We have fitted our calculated mean static polarizabilities per atom $\bar{\alpha}_{at}$ to an expression given by [40]

$$\bar{\alpha}_{at} = \frac{(n^{1/3}r_{WS} + \delta)^3}{n}, \tag{5}$$

where r_{WS} is the Wigner-Seitz radius and δ represents the spillout of the electrons from the surface of a metallic sphere. The values of the parameters resulting from the fitting to Eq. (5) are $r_{WS} \approx 1.63$ Å and $\delta \approx 0.45$ Å which are close to the values $r_{WS} \approx 1.58$ Å and $\delta \approx 0.79$ Å reported in Refs. [41,1], respectively. The bulk limit of Eq. (5) predicts a value for the bulk atomic polarizability of 4.33 Å³/atom that is lesser than those of the alkali metals like for example Na which is around 9 Å³/atom [42]. As commented above, it is due to the ever increasing role of the *d* electrons since that the screening of *d* electrons (core polarization) tends to reduce the polarizability. Despite the fact that the jellium model in the spillout approximation predicts on average the trend of the polarizability per atom in function of the cluster size, it cannot account for the more interesting quantum mechanical effects. Thus deviations of the calculated polarizabilities from the predictions of Eq. (5) are "true" quantum effects. As commented above, it is in part due to the shell effects.

In Table II, we have collected the numerical values of the disproportionation energy, that is defined as

$$\Delta_2 E_n = E_{n+1} + E_{n-1} - 2E_n, \tag{6}$$

where E_n is the total energy provided by our DFT calculations of the cluster with *n* atoms. It represents the relative stability of a cluster with *n* atoms in comparison to clusters with $n+1$ and $n-1$ atoms and consequently a peak in $\Delta_2 E_n$ indicates that the cluster with size *n* is very stable because a shell has been filled. The disproportionation energy shows that clusters with $n=2$, 8, and 18 have particularly stable configurations and consequently the polarizability is considerably reduced, as is shown in Fig. 2. Whenever a shell starts to fill, the polarizability increases and deviates from the jellium model. As the size of the silver clusters increases, the

HOMO-LUMO gap becomes smaller (see Table II) so that the shell effects are less important and the deviation of the jellium model is negligible.

V. SUMMARY

In this article the structural stability along with the static response properties of silver clusters in the size range $1 \leq n \leq 23$ have been studied by means of the finite field method implemented in the Kohn-Sham density-functional methodology [12]. The IPs reported in this article for the lowest-energy structures are in general in relatively good agreement with the experimental measurements and most of the structures predicted in this article as the fundamental ones were already reported in former publications. Likewise, the calculated polarizabilities are in good agreement with the experimental measurements reported in Ref. [35]. The competition between the HOMO-LUMO gap and the structural symmetry on one side or the shell structure and the disproportionation energy on the other side are the quantum-mechanical effects that deviate the calculated polarizabilities from the jellium model. For bigger cluster sizes the quantum-mechanical effects can be considered of less importance, and therefore both theoretical approaches, i.e., the *ab initio* DFT calculations and the jellium model, approach each other.

ACKNOWLEDGMENTS

APPENDIX: HELLMANN-FEYNMAN THEOREM

The purpose of this appendix is to show that the finite basis set GGA calculation holds the Hellmann-Feynman theorem when fully converged in the framework of density functional theory [43]. We have restricted ourselves for brevity of the formulas to wave functions without spin polarization; however, this is not a substantial restriction and the extension to spin-unrestricted orbitals is straightforward.

We have selected the ansatz in which the Kohn-Sham orbitals $\psi_i(r)$ are represented by linear combinations of atomic Gaussian-type orbitals $\chi_j(r)$. Thus the orthonormal Kohn-Sham orbitals are given by

$$\psi_i(r) = \sum_j c_{ij}\chi_j(r), \tag{A1}$$

where c_{ij} are the corresponding molecular orbital coefficients. With this expansion we find the following relation for the electronic density:

$$\rho(r) = \sum_{i,j} P_{ij}\chi_i(r)\chi_j(r), \tag{A2}$$

where P_{ij} represents an element of the density matrix, defined as $P_{ij}=2\Sigma_k^{occ}c_{ik}c_{jk}$. Using Eq. (A1) for the LCGTO expansions of the Kohn-Sham orbitals subject to the orthonor-

malization condition and the electronic density described in Eq. (A2), the variationally minimized Kohn-Sham SCF energy expression may be written after some manipulation as

$$E_{SCF}(\lambda) = \sum_{ij} P_{ij} H_{ij}(\lambda) + \frac{1}{2} \sum_{ijkl} P_{ij} P_{kl} (ij|kl)(\lambda)$$
$$- 2 \sum_{ijk} \epsilon_k [c_{ki} c_{jk} S_{ij}(\lambda) - 1] + E_{XC}(\rho(\lambda), \nabla\rho(\lambda)),$$

$$(A3)$$

where H_{ij} represents the matrix elements of the core Hamiltonian and they are built from the kinetic and electron-nuclear interaction energies. The second term represents the Coulomb repulsion energy of the electrons and the term E_{XC} is the XC energy in the GGA. We use the notation $(ij|kl) = \int\int \psi_i(1)\psi_j(1)(1/r_{12})\psi_k(2)\psi_l(2)dr_1 dr_2$, and λ is any parameter at all which affects the Hamiltonian of the system. The quantities ϵ_k are one-electron eigenvalues for the occupied orbitals and S is the overlap matrix defined as $S_{ij} = \langle\chi_i|\chi_j\rangle$.

Assuming a gradient-corrected form for the XC energy $E_{XC} = \int g(\rho, |\nabla\rho|^2)dr$ and upon differentiation of the energy with respect to λ we find

$$\nabla_\lambda E = \sum_{ij} P_{ij} \nabla_\lambda H_{ij} + \frac{1}{2} \sum_{ijkl} P_{ij} P_{kl} \nabla_\lambda (ij|kl) - 2 \sum_{ijk} \epsilon_k c_{ki} c_{jk} \nabla_\lambda S_{ij}$$
$$+ \sum_{ij} P_{ij} \left(\langle \nabla_\lambda i | E_{XC} | j \rangle + \langle i | E_{XC} | \nabla_\lambda j \rangle + \left\langle i \left| \frac{\partial g}{\partial \rho} \nabla_\lambda \rho \right| j \right\rangle \right.$$
$$\left. + 2 \left\langle i \left| \frac{\partial g}{\partial |\nabla\rho|^2} \nabla_\lambda (|\nabla\rho|) \right| j \right\rangle \right). \quad (A4)$$

The XC contribution to the derivative of the energy involves derivatives of the wave function either explicitly or implicitly throughout the electronic density. Denoting a_i as a parameter of the wave functions that can be an exponent or positions of the basis functions, the functional derivative of the wave function can be written as $|\nabla_\lambda i\rangle = |\partial i / \partial a_i\rangle (da_i/\lambda)$. Thus we can optimize all parameters a_i so that the derivative of the XC energy can be neglected as well as the two-electron contribution of the Hamiltonian operator of Eq. (A3). Considering that the overlap matrix is independent of the perturbation λ as, for example, in the case of a uniform external electric field, the third term depending on the derivative of the overlap matrix vanishes. Consequently,

$$\nabla_\lambda E = \langle \nabla_\lambda H \rangle, \quad (A5)$$

which means that the fully self-consistent finite basis set solutions satisfy the Hellmann-Feynman theorem in the framework of DFT when the XC energy is approximated by the GGA implementation.

[1] W. A. de Heer, Rev. Mod. Phys. **65**, 611 (1993).

[2] M. Brack, Rev. Mod. Phys. **65**, 677 (1993).

[3] F. Baletto and R. Ferrando, Rev. Mod. Phys. **77**, 371 (2005).

[4] Q. A. Pankhurst, J. Connolly, S. K. Jones, and J. Dobson, J. Phys. D **36**, R167 (2003).

[5] U. Kreibig and M. Vollmer, *Optical Properties of Metal Clusters* (Springer, Berlin, 1995).

[6] K. Deng, J. Yang, and C. T. Chan, Phys. Rev. A **61**, 025201 (2000).

[7] I. Moullet, J. L. Martins, F. Reuse, and J. Buttet, Phys. Rev. Lett. **65**, 476 (1990).

[8] J. C. Idrobo, S. Ogut, and J. Jellinek, Phys. Rev. B **72**, 085445 (2005).

[9] H. A. Kurtz, J. J. P. Stewart, and K. M. Dieter, J. Comput. Chem. **11**, 82 (1990).

[10] I. Vasiliev, S. Ogut, and J. R. Chelikowsky, Phys. Rev. Lett. **78**, 4805 (1997).

[11] J. Zhao, J. Yang, and J. G. Hou, Phys. Rev. B **67**, 085404 (2003).

[12] A. St-Amant and D. R. Salahub, Chem. Phys. Lett. **169**, 387 (1990), http://www.demon-software.com/public_html/.

[13] J. P. Perdew and Y. Wang, Phys. Rev. B **46**, 12947 (1992).

[14] M. Pereiro, D. Baldomir, M. Iglesias, C. Rosales, and M. Castro, Int. J. Quantum Chem. **81**, 422 (2001).

[15] B. Simard, P. A. Hackett, A. M. James, and P. R. R. Langridge-Smith, Chem. Phys. Lett. **186**, 415 (1991).

[16] S. Huzinaga *et al.*, *Gaussian Basis Sets for Molecular Calculations* (Elsevier, Amsterdam, 1984).

[17] L. Versluis and T. Ziegler, J. Chem. Phys. **88**, 322 (1988).

[18] H. B. Schlegel, *Modern Electronic Structure Theory* (World Scientific, Singapore, 1995), Chap. 8, p. 459.

[19] R. Fournier, J. Chem. Phys. **115**, 2165 (2001).

[20] S. Chretien and D. R. Salahub, Phys. Rev. B **66**, 155425 (2002).

[21] The Cambridge Cluster Database, http://www-wales.ch.cam.ac.uk/CCD.html.

[22] E. R. J. Andzelm and D. R. Salahub, J. Chem. Phys. **83**, 4573 (1985).

[23] J. Zhao, Y. Luo, and G. Wang, Eur. Phys. J. D **14**, 309 (2001).

[24] V. Bonacic-Koutecky, L. Cespiva, P. Fantucci, and J. Koutecky, J. Chem. Phys. **98**, 7981 (1993).

[25] Z. F. Liu, W. L. Yim, J. S. Tse, and J. Hafner, Eur. Phys. J. D **10**, 105 (2000).

[26] J. A. Howard, R. Sutcliffe, and B. Mile, Surf. Sci. **156**, 214 (1985).

[27] T. L. Hasiett, K. A. Bosnick, and M. Moskovits, J. Chem. Phys. **108**, 3453 (1998).

[28] C. Jackschath, I. Rabin, and W. Schulze, Z. Phys. D: At., Mol. Clusters **22**, 517 (1992).

[29] During the geometry optimization process, the structure consisting of five atoms forming a pentagon and with the other atom in the center of it converged to the pentagonal pyramid. Therefore, we have decided to strip off any information about this structure because it is the same as the pentagonal pyramid.

[30] V. Bonacic-Koutecky, V. Veyret, and R. Mitric, J. Chem. Phys. **115**, 10450 (2001).

[31] K. LaiHing, P. Y. Cheng, and M. A. Duncan, Z. Phys. D: At., Mol. Clusters **13**, 161 (1989).

[32] M. Pereiro, and D. Baldomir, Phys. Rev. A **72**, 045201 (2005).

[33] K. Michaelian, N. Rendón, and I. L. Garzón, Phys. Rev. B **60**, 2000 (1999).

[34] S. Erkoç and T. Yilmaz, Physica E (Amsterdam) **5**, 1 (1999).

[35] S. Fedrigo, W. Harbich, J. Belyaev, and J. Buttet, Chem. Phys. Lett. **211**, 166 (1993).

[36] C. J. F. Bottcher, *Theory of Electric Polarization* (Elsevier, Amsterdam, 1973), Chap. 5, p. 165.

[37] C. Kittel, *Introduction to Solid State Physics* (Wiley, New York, 2005), Chap. 1, p. 20.

[38] P. Calaminici, A. M. Koster, A. Vela, and K. Jug, J. Chem. Phys. **113**, 2199 (2000).

[39] M. J. Puska, R. M. Nieminen, and M. Manninen, Phys. Rev. B **31**, 3486 (1985).

[40] D. R. Snider and R. S. Sorbello, Phys. Rev. B **28**, 5702 (1983).

[41] L. H. Bennett, R. W. Mebs, and R. E. Watson, Phys. Rev. **171**, 611 (1968).

[42] G. Tikhonov, V. Kasperovich, K. Wong, and V. V. Kresin, Phys. Rev. A **64**, 063202 (2001).

[43] *Modern Electronic Structure Theory*, edited by D. R. Yarkony (World Scientific, Singapore, 1995), Vol. II, p. 1191.